

# A Wavelet-CNN-LSTM Model for Tailings Pond Risk Prediction

Jun Yang<sup>1,2,\*</sup>, Qing Li<sup>1</sup>, and Yixuan Sun<sup>2</sup>

**1** National and Local Joint Engineering Laboratories for Disaster Monitoring Technologies and Instruments, China Jiliang University, Hangzhou 310018, China

**2** National and Local Joint Engineering Laboratories for Disaster Monitoring Technologies and Instruments, China Jiliang University, Hangzhou 310018, China

**3** Department of Mechanical Engineering, Purdue University, West Lafayette, IN 47907, USA

\* correseponding@junyang-0309@hotmail.com

## Abstract

Tailings ponds are places for storing industrial waste. Once the tailings pond collapses, the villages nearby will be destroyed and the harmful chemicals will cause serious environmental pollution. There is an urgent need for a reliable forecast model, which could investigate the variation trend of stability coefficient of tailing dam and issue early warnings. In order to fill the gap, this work presents an hybrid network - Wavelet-based Long-Short-Term Memory (LSTM) and Convolutional Neural Network (CNN), namely Wavelet-CNN-LSTM netwrok for predicting the tailings pond risk. Firstly, we construct the especial nonlinear data processing method to impute the missing value with the numerical inversion (NI) method, which combines correlation analysis, sensitivity analysis, and Random Forest (RF) algorithms. Secondly, a new forecasting model was proposed to monitor the saturation line, which is the lifeline of the tailings pond and can directly reflect the stability of the tailings pond. After using the discrete wavelet transform (DWT) to decompose the original saturation line data into 4-layer wavelets and de-noise the data, the CNN was used to identify and learn the spatial structures in the time series, followed by LSTM cells for detecting the long-short-term dependence. Finally, different experiments were conducted to evaluate the effectiveness of our model by comparing it with other state-of-the-art algorithms. The results show that Wavelet-CNN-LSTM achieves the best score both in mean absolute percentage error (MAPE), root-mean-square error (RMSE) and  $R^2$ .

## Introduction

Tailings ponds are places for storing industrial waste. The tailings pond failure is ranked 18th in the world's risk assessment [8]. Worldwide, at least 84 major tailings dam accidents were reported that caused significant damage from 1960–2020 [1]. Nowadays, the safety performance of tailings ponds can only be obtained by manual observation or measurement analysis from specific sensors. The measurement includes the saturation line, displacement and deformation of the dam body, seepage flow, and dry beach length.

---

In practice, considering the variability of topography, weather, and mine construction conditions, the stability of the tailings dam is very complicated and changeable.

At present, a large number of researchers are devoted on tailings pond monitoring [2, 14, 26, 41, 42]. The researchers are mainly focusing on the stability status by monitoring data from sensors and make early-warnings in time by mathematical modeling method, image recognition method and data analysis. Huang et al. [3] conducted a tailings pond monitoring and early-warning system based on three-dimensional GIS, the response time of the safety monitoring and early warning system is less than 5 seconds. Li et al. [5] proposed GPS means to monitor the displacement of tailings dam online. Gao et al. [6] established remote sensing interpretation using high-resolution remote sensing images. M.Necsoiu [7] used satellite radar interferometry to monitor the tailings sedimentation. D.F.Che et al. [8] assessed the risk of tailings pond by runoff coefficient, which can simultaneously determine the safety performance of multiple tailings dams. Dong et al. [10] set up the alarm system based on the cloud platform, showing good performance in real-time monitoring. Qiu et al. [11] designed a monitoring system of saturation line based on mixed programming.

Tailings dams are usually located in remote mountainous areas, the structure is very complicated and the dam breaks problems are almost nonlinear. As a result, the stability of the tailings pond cannot be directly observed. Recently, with the advantages of handling almost any non-linear and linear problems whatever low- and high-dimensions, neural network and machine learning methods have been effectively composed in real-time risk analysis and evaluation [4, 9, 12, 19, 43–46]. However, the role of real-time monitoring cannot be equated with early warning and forecasting. In other words, risk prediction methods could help people perceive risk before it happens. With excellent ability to process time-series, classic prediction model such as Auto-Regressive Integrated Moving Average (ARIMA) and LSTM have been used in prediction problems [21, 28, 47–49]. They analyze and identify the time series information of training data and give the prediction value for a few days in advance. Nevertheless, different from LSTM, the ARIMA model only gets a high score at the condition of data with linear correlation or without obvious fluctuation. With the rapid development of deep learning, the CNN and LSTM have been the most popular networks. The CNN could filter out the noise data and extract important features, achieving good performance in images, speech, and time-series [50, 51]. While the LSTM network has the ability to find the linear or nonlinear time series information from the shallow and deep network and combine it with current memory [52]. In light of this, combining LSTM with CNN may achieve better prediction performance to a large extent.

As the most important factor of stability of tailings dams, for every 1-meter drop in saturation line, the safety factor of static stability is increased by 0.05 or more [11]. High saturation line will lead to a decrease of the dam stability and even potentially causing leakage, landslide, and dam break [32–34]. Therefore, the saturation line is called the lifeline of tailings dams [13]. Therefore, the stability of tailings dam can be determined by their saturation line position of tailings dam accurately. It is imperative to establish accurate models to predict the height of saturation line and the security situation of tailings ponds. However, the prediction research of tailings pond is almost nonexistent. For this purpose, our goal is to propose a new model that can make full use of the strengths of deep learning. In more detail, utilizing the hidden information of the previous saturation line, the model will predict the value and tendency in the next few days. Meanwhile, our proposed model is evaluated by comparing with state-of-the-art models, which shows our two kinds of CNN-LSTM models are the most effective choice, especially the *CNN – LSTM<sup>2</sup>*. Where convolutional layers play important roles in grabbing more complex information and pass it on to the LSTM layers. It should be mentioned that because of the complex situation of the tailings dam, the data sequence

of the saturation line is unstable and there is a lot of noise. whether in terms of time or frequency of data, the noises usually contain useless information, which not only takes up a lot of space or memory, but also affects the analyst to draw accurate conclusions. To overcome the drawbacks of simple networks that cannot de-noise the raw data, we applied the discrete wavelet transform (DWT) to decompose the saturation line into different time-frequency sequences, and the rigorous strategy is used to calculate threshold to remove the noise in the decomposed data, and finally the de-noised wavelet is reconstructed to obtain new integrated data for further study. Combining the DWT method, our  $CNN - LSTM^2$  can be improved as Wavelet-CNN-LSTM to achieve the better performance. In this work, taking Jiande tailings pond, China, as the study area, four main contributions of our study are presented:

- (1) Proposing a NI method using RF algorithm to fill missing values, which save the time-series information as much as possible.
- (2) Proposing a new CNN-LSTM network to solve the tailings pond risk prediction problem, which achieves great performance in MAPE, RMSE and  $R^2$ .
- (3) Comparing our CNN-LSTM model with different hyperparameters and with other state-of-the-art algorithms.
- (4) Combining the DWT method with CNN-LSTM network to achieve better performance, especially in data with a lot of noise.

Totally, in this work, Pearson correlation coefficient, feature importance of RF model and sensitivity analysis techniques have been employed for the saturation line prediction, especially served as tools of dimensionality reduction. After the process of dimensionality reduction, only two kinds of monitoring data are needed to restructure the saturation line data. After de-noise the data using DWT, our Wavelet-CNN-LSTM model was established for further tailings pond risk forecast.

## Materials and Methods

### Numerical Inversion Method

In the monitoring data, a small part of the data is missing or abnormal. It should be noticed that, for a time-series prediction problem, missing value will cause the loss of time dependence, which will restrict the performance of the prediction model [17, 18, 29, 30]. Hence, we hope to keep our data with favourable long-term and short-term continue information. Similarly, instead of deleting the abnormal data directly, abnormal saturation line value could be reconstructed by our NI system. The key to the solution is to find the relationship between missing value and other normal values. According to the special relationship, the missing value could be reconstructed by other normal values. However, it is hard to find the precise computing relationship between the saturation line values and other features. The method in this study is to create a direct mapping from the inputs to the outputs, using machine learning, which has the ability for finding the relationship between inputs and outputs [16].

In other words, we composed our NI method to reconstruct the data from building the RF model, by doing so, more data are achievable. In more detail, this NI system includes three steps. First, considering that a large number of parameters may have a strong correlation and if the correlation among features is strong, it will be difficult to evaluate the importance of a single feature. Taking into account the possibility of missing values for each parameter, we should choose as few parameters as possible as the input of NI method. To solve the problem, Pearson correlation coefficients [38, 39] are calculated and a heat map is drawn, which helps eliminate the characteristics with a strong correlation (correlation coefficient greater than 0.8). The Pearson correlation

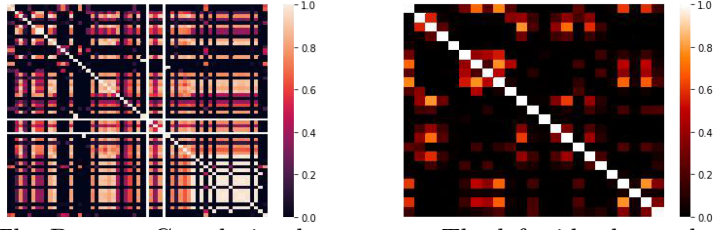


**Figure 1.** The Pearson Correlation heat maps. The left side shows the correlations among original data, the right side shows the correlations among the remaining features.

coefficients is defined as follows:

$$P_{m_i, n_i} = \frac{k \sum m_i n_i - \sum m_i \sum n_i}{[k \sum m_i^2 - (\sum m_i)^2]^{\frac{1}{2}} [k \sum n_i^2 - (\sum n_i)^2]^{\frac{1}{2}}} \quad (1)$$

where  $m_i, n_i$  are two different variables,  $k$  is the number of variables. From Figure 1, the left side shows the correlations among original data, the right side shows the correlations among the remaining features by Pearson method. Second, a RF model has been composed, where we explored the feature importance ranking generated by RF [22, 31] by sorting the features according to how much they contributed to the model during building process. Third, posterior judgment is also required. We are interested in which features have great impacts on the output of the trained RF model. Sobol sensitivity analysis is adopted to explore the contribution of the individual feature and which parameters are influential and drive model outputs [23–25, 39]. The feature importance ranking according to the RF model and sensitivity analysis are shown in Figure 2. They jointly selected  $x_3$  (rainfall) and  $x_4$  (water level) as the most important parameters. Subsequently, RF is used to create a direct mapping finding the linear and nonlinear relationship between inputs ( $x_3, x_4$ ) and outputs (saturation line) to predict the saturation line [16]. Moreover, the abnormal data will be deleted and replaced with predicted data by NI method. It should be noticed that rainfall and water level are factors that directly affect the height of the saturation line, and they have a similar time-series relationship. Therefore, the NI method in this study greatly preserves the time-series information of the saturation line and generate more achievable values for further deep learning prediction.

## Discrete Wavelet Transform

Although the window Fourier transform (short-time Fourier transform) can partially locate the time, since the window size is fixed, it is only suitable for stationary signals with small frequency fluctuations, and not suitable for non-stationary signals with large frequency fluctuations. As a signal time-frequency analysis method, the wavelet transform (WT) can automatically adjust the window size according to the frequency. What has greatly contributed the effectiveness of WT is the truth that it is an adaptive time-frequency analysis method which can perform multi-resolution analysis. As a very suitable non-stationary signals method, local features of signals can be extracted by WT. As a result, wavelet transform is known as a microscope for analyzing and processing signals. In our study, we apply the discrete wavelet transform (DWT) [26] to decompose the collected saturation line data of tailings pond in to 4 frequency sequences. After removing the noise in the decomposed data, the wavelets are reconstructed to obtain new integrated data for further multi-resolution study. The WT refers to the displacement of a certain basic wavelet function by  $\omega$  units, and then the inner product with the analysis signal  $p(t)$  at different scales.

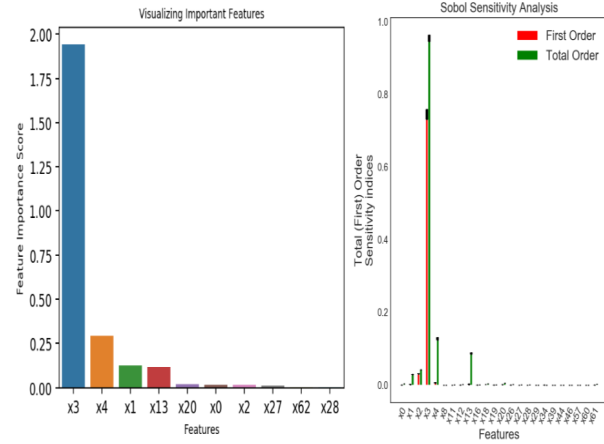


**Figure 2.** The feature importance ranking according to the RF model(left) and sensitivity analysis(right). It means that in the RF model we trained,  $x_3$  (rainfall) and  $x_4$  (water level) are the most important, which shows that only the values of rainfall and water level are needed to get the corresponding infiltration line value.

$$WT_s(\epsilon, \omega) = \frac{1}{\sqrt{n}} \int_{-\infty}^{+\infty} p(t) \phi\left(\frac{t - \omega}{n}\right) dt \quad (2)$$

where  $\epsilon$  is the scale factor (larger than 0), which is used to stretch the each basic wavelet  $\phi(t)$ .  $\omega$  is the displacement. Mallat algorithm [23] provides an effective way to display DWT to process the data using the low-high-pass filters:

$$oL = \sum_{i=-\infty}^{\infty} T(i) \psi_l(2n - i) \quad (3)$$

$$oH = \sum_{i=-\infty}^{\infty} T(i) \psi_h(2n - i) \quad (4)$$

Where  $T(i)$  means the signal.  $\psi_l$ ,  $\psi_h$ ,  $oL$ ,  $oH$  are the low-pass filter, high-pass filter, output of low-pass filter, and output of high-pass filter, respectively. Notably, In the wavelet domain, the coefficient corresponding to the effective signal is large, and the coefficient corresponding to the noise is small, the *rigrsure* threshold is an effective way in DWT:

$$g(k) = [sort|t|]^2, \quad (k = 0, 1, \dots, N - 1) \quad (5)$$

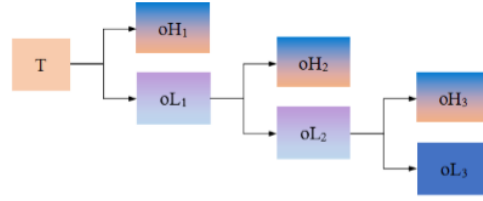
In the equation, the absolute value of each signal is achieved and then sorted, and the square of each number is taken to obtain a new signal sequence.

$$\gamma_t = \sqrt{g(k)}, \quad (t = 0, 1, \dots, N - 1) \quad (6)$$

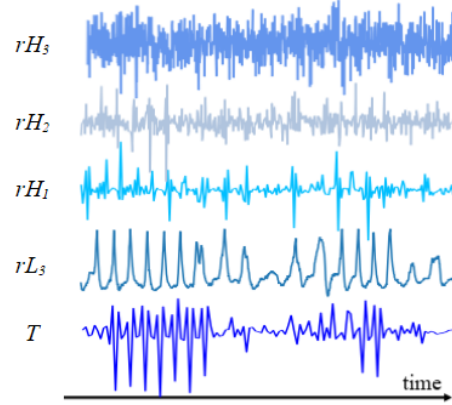
$$Risk(t) = \frac{(N - 2t + \sum_{i=1}^t g(j) + (N - t)f(N - t))}{N} \quad (7)$$

$$\gamma_t = \sqrt{g(t_{min})} \quad (8)$$

The  $t$  is the signal,  $\gamma_t$  is the threshold and  $Risk(t)$  is the generated risk. Take the minimum  $g(t)$  corresponding to all risks  $r(K)$  to get the final threshold  $\gamma_t$ .



(a) The decomposition process.



(b) The reconstruction process.

**Figure 3.** The Discrete Wavelet Transform process.

The 3-level decomposition and the reconstruction process of DWT using Mallat algorithm is shown in Figure 3(a) and Figure 3(b), respectively. From Figure 3(a) we can see that after decomposing the signal into three different levels. In more detail, at the first level, the original signal  $T$  is decomposed to the detail coefficients  $oL_1$  and  $oH_1$ . Then the achieved  $oL_1$  is decomposed to the other two coefficients  $oH_2$  and  $oL_2$  at the second level. The decomposition process does not end until the set number of  $n$ -level steps is reached. The Figure(b) illustrates the process of de-noise and reconstruction. The noises are shown with small wavelet coefficients, while the useful signals are shown with small wavelet coefficients [35, 36]. The time-series signal  $T$  passes through the low-pass filter  $oL_1$  and high-pass filter  $oH_1$  for removing the wavelet coefficients of lower amplitude and restore the wavelet coefficients of higher amplitude to achieve the effect of noise reduction. Subsequently the wavelet reconstruction and integration process is applied on all of these coefficients. Employing the coefficient  $oL_3$ , the low frequency and high amplitude  $rL_3$  is reconstructed. As shown in  $rL_3$  in Figure(b), the sequences become smooth, showing the more obvious tendency change patterns.

## CNN-LSTM Prediction Model

Our study aims to develop the construction of a prediction system for forecasting the saturation line utilizing state-of-the-art LSTM and CNN networks. What has devoted to the popularity of the convolutional layer is the fact that it good at extracting and recognizing as well as identifying the structures of the time series in the monitoring data, while the LSTM networks achieve good performance in detecting long-short-term dependence. In light of this, the principle idea of our study is to combine the advantages of CNN and LSTM.

The proposed model in our study named CNN-LSTM model, including two versions, which include two parts of layers. The first part is convolutional layers and max-pooling

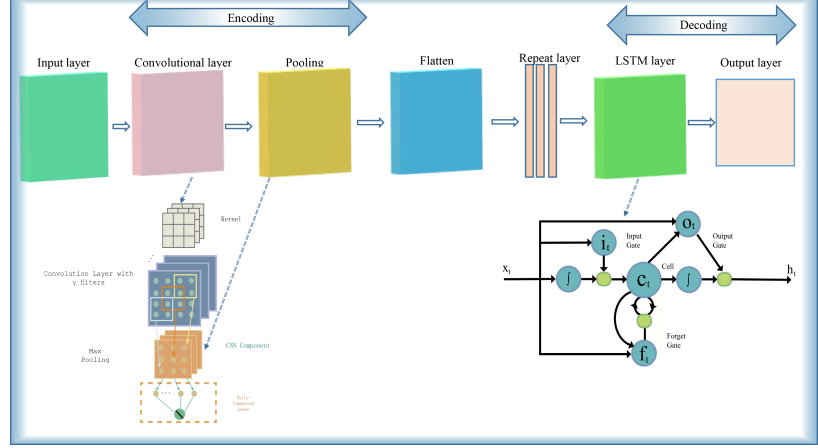


Figure 4. The CNN-LSTM auto-encoder model.

layers, while the second part is LSTM layers. The convolutional layers encode the time-series information, while the LSTM layer decodes the encoded information from convolutional layers, and will be flatten and pushed into a fully-connected layer. The CNN-LSTM auto-encoder model is shown in Figure 4.

### Convolutional and Pooling Layers

The convolutional layers and the max-pooling layer detect the spatial structures and features of the saturation line values together with reducing the redundant characteristics, respectively. More important, the convolutional layer could extract hidden information in the time dimension, and usually passes higher quality and denser features to further layers.

More specifically, numerous useful convolved features will be generated by convolution kernels, which are always more important than the original features. As a subsampling method, max-pooling layer saves certain information from the convolved features and reduce the original data dimension. Specifically, the pooling layer helps to collect and summarize the features from convolutional layer.

### Long-Short-Term Memory (LSTM) network

As a popular type of recurrent neural network(RNN), LSTM achieves good performance in detecting long-term dependencies. The problem named "lack of memory" was solved after LSTM was proposed, which means the time-series information cannot be effectively exhibited. Moreover, "vanishing gradient problem" prevents the RNN for long-time dependencies detecting. The LSTM model is composed of one memory unit and other three interactive gates: memory cell, input gate, forget gate and output gate. The memory cell memorizes the state from the previous state. The input gate determines how much input data of the network needs to be saved to the unit state at the current moment  $t$ . The forget gate controls whether the information will be discarded or enters the input gate as reserved information at time  $t - 1$ . The output gate determines what information will be utilized as the output. Eqs.(1)–(6) briefly describe the update in the LSTM layers.

$$i_t = \sigma(V_i x_t + W_i h_{t-1} + b_i) \quad (9)$$

$$f_t = \sigma(V_f x_t + W_f h_{t-1} + b_f) \quad (10)$$

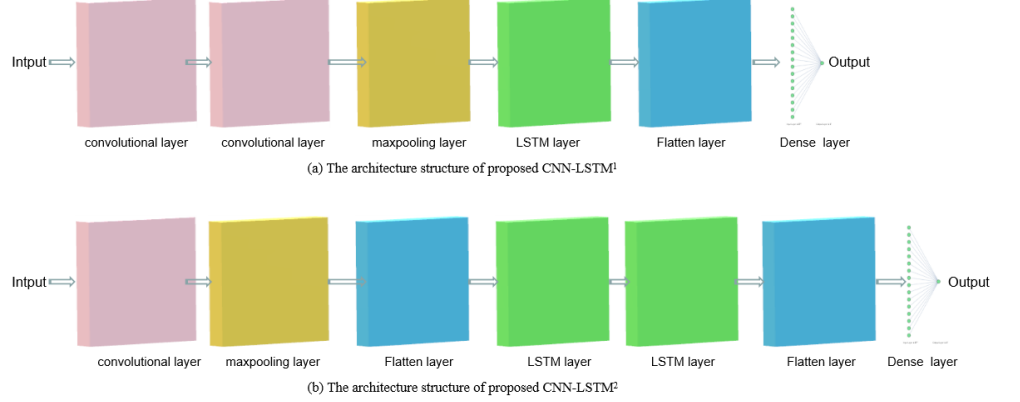


**Figure 5.** The architecture structure of proposed  $CNN-LSTM^1$  and  $CNN-LSTM^2$

$$\tilde{c}_t = \tanh(V_c x_t + W_c h_{t-1} + b_c) \quad (11)$$

$$c_t = f_t \otimes c_{t-1} + i_t \otimes \tilde{c}_t \quad (12)$$

$$o_t = \sigma(V_o x_t + W_o h_{t-1} + b_o) \quad (13)$$

$$h_t = o_t \otimes \tanh(c_t) \quad (14)$$

where  $x_t$  is the input data at time  $t$ ,  $V_*$  and  $W_*$  denote the weight matrix,  $h_*$  is the hidden state,  $b_*$  is the bias.  $\sigma$  and  $\tanh$  are the activation function of sigmoid and tanh, respectively.  $i_t, f_t, c_t$  and  $o_t$  stand for the input gate, forget gate, memory cell and output gate, respectively. The  $\otimes$  means the component-wise operation. Finally, output  $h_t$  is calculated by output gate and information in memory cell.

### CNN-LSTM Model For Prediction

In our study, two different CNN-LSTM structures are utilized. The first version named  $CNN-LSTM^1$ , which consists of two convolutional layers of 16 and 32, a max-pooling layer filters of 2, a LSTM layer of 50, a flatten layer and a fully-connected layer in order. The second version named  $CNN-LSTM^2$ , which includes one convolutional layer filters of 32, a max-pooling layer filters of 2, a flatten layer, two LSTM layers of 25, 50, a flatten layer and a fully-connected layer in order. Different parameters are compared for further study. The two kinds of CNN-LSTM structures are shown in Figure 5(a) and Figure 5(b).

### Data Preparation

The study site is Jiande copper mine tailings pond, Hangzhou, Zhejiang Province, China, where the amount of mineral copper metal accounts for about 60% of the province's total output. The main mineral products are copper concentrate, zinc concentrate, sulfur concentrate, and by-product gold and silver. The tailings pond level is *III*. Different geological hazard sensors are installed to monitor the surface displacement, dam body internal displacement, saturation line height, water level, rainfall, and seepage flow [26, 27, 37]. The research data for this work were collected from the sensors mentioned above from 2018-03-18 to 2019-04-29. For this study, our

**Table 1.** Describe of the datasets used for saturation line prediction.

	NO.8	NO.13	NO.17	NO.21	NO.28	NO.33	Base status
1	4.56	7.78	11.38	10.76	14.10	15.01	Normal
2	4.58	7.79	11.35	10.72	14.16	15.07	Normal
3	4.59	7.81	11.37	10.81	14.18	15.27	Normal
—	—	—	—	—	—	—	—
mean	4.57	7.73	11.32	10.67	14.52	15.03	Normal
min	4.08	6.86	11.14	10.08	14.04	14.70	Normal
25%	4.51	7.68	11.28	11.28	14.23	14.96	Normal
50%	4.56	7.80	11.36	10.76	14.61	15.01	Normal
75%	4.61	7.84	11.37	10.80	14.68	15.04	Normal
max	4.95	8.18	11.40	10.88	15.40	15.41	Normal

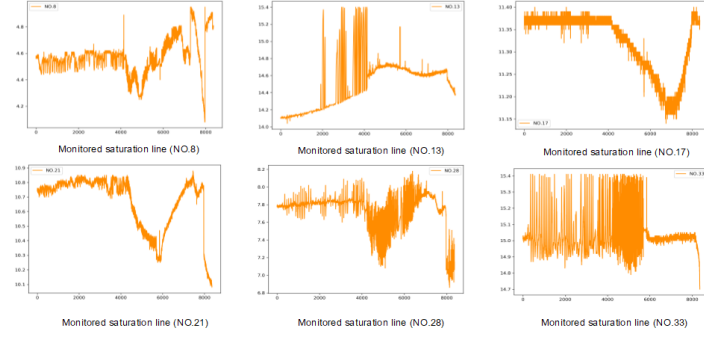


**Figure 6.** The monitored saturation line data at different positions

data are from 5 different positions, specifically the 8, 13, 17, 21, 28, 33 stage of the tailings dam, and the time interval between data is two hours.

After collecting the data, we used our proposed NI system to fill the missing value and the abnormal value will be deleted and replaced with predicted value by NI system. Finally, 8365 data were collected for our further study. The continuous monitoring value ensures a wide range of time-series information. It should be noted that our CNN-LSTM model trained and validated on the 8365 data. Among the 8365 data, we randomly choose 70% of the data as the training sets, the 10% as the validation set. The performance of the models was evaluated on the rest 20% data, which is the unseen part during the model building process. For keeping the long-short-term dependence in the data, these data cannot be shuffled as usual in traditional deep learning studies. Table 1 shows the describe of the collected data, and the first three rows are historical monitoring data. The distribution of monitoring data is shown in Figure 6. As is shown in Figure 6, there is a wide range of variation in the monitoring data. These changes are largely affected by tailings pond operations and weather change, such as the discharge of a large amount of wastewater and waste residue on a certain day or the experience of heavy rain.

In order to eliminate the impact of different data dimensions on the calculation, we used  $Z - score$  normalization on the data, the formula is as follows:

$$\dot{x} = \frac{x_t - \mu_t}{\sigma_t} \quad (15)$$

where  $x_t$  is the input data,  $\mu_t$  and  $\sigma_t$  are the averages and standard deviation of data.

---

## Experiment and Results

Two different version  $CNN - LSTM^1$  and  $CNN - LSTM^2$  are evaluated and compared to show the prediction performance. The simulation hardware environment of this experiment is Intel Core CPU i7-8750. GPU is NVIDIA GTX 1060, and the memory is 6GB. The algorithm is implemented using Python in conjunction with the TensorFlow framework.

### Experiment and Results using CNN-LSTM model

The prediction performance of our proposed model is evaluated by root mean square error (RMSE). In fact, RMSE meets an important problem: let us consider that although the model has an error of less than 0.5% in the 98% dataset and very big error in the other 2% dataset, the overall RMSE will be still very high, resulting in this model considered as a poor model. To solve this problem, mean absolute percentage error (MAPE) is utilized in the evaluation process. What's more, coefficient of determination, denoted as  $R^2$ , is also used in our evaluation methodology. It is the proportion of the total variation of the dependent.

$$RMSE = \left[ \frac{1}{n} \sum_{i=1}^n (y_t - \hat{y}_p)^2 \right]^{\frac{1}{2}} \quad (16)$$

$$MAPE = \sum_{i=1}^n \frac{\left| \frac{y_t - \hat{y}_p}{y_t} \right| * 100\%}{n} \quad (17)$$

$$R^2 = 1 - \frac{\sum_{i=0}^n (y_t - \hat{y}_p)^2}{\sum_{i=0}^n (y_t - \bar{y}_t)^2} \quad (18)$$

Where  $y_t$  represents the true value,  $\hat{y}_p$  represents predicted saturation line value,  $\bar{y}_t$  represents average of true value, and  $n$  is the count of data. Figure 7 shows the prediction results of  $CNN - LSTM^1$  and  $CNN - LSTM^2$  on five different monitoring sites about 1750 test sets.

In this study, we trained our model for 120 epochs with a batch size of 64, RMSE as loss function and Adam for optimizer. The Adam is an improved RMSProp optimizer combining with the moments trick. It is worth noticing that in order to reduce the feature loss during the convolutional layers, same padding operation was conducted during this process. The last but not least, the forecasting sequence length should be set properly to make sure the model performance. Specifically, we set the sequence length as 10. On the one hand, considering that a longer sequence length will occupy a huge computer memory, on the other hand, we found through experiments that set the sequence length to 10 achieves better performance than, for example, 4, 7, 20. The most important thing for the hyperparameter selection of the model is the learning rate of the network, which has a significant influence on time consumption until convergence. If the learning rate is set too large, the loss function will be difficult to converge, resulting in a lower final detection accuracy; On the contrary, a small learning rate will lead to slow convergence and increase the training time. This paper uses cross-validation to determine the optimal learning rate for each partial network, and the most appropriate optimal learning rate is 0.001 and weight decay is 0.005. For the selection of the number of network iterations, the training process is stopped when the model no longer converges.

The prediction performance of our proposed  $CNN - LSTM^1$  and  $CNN - LSTM^2$  are shown in Table 2 and Table 3, respectively. NO.8, NO.13, NO.17, NO.21, NO.28, NO.33 means the different station of saturation line mentioned above. The

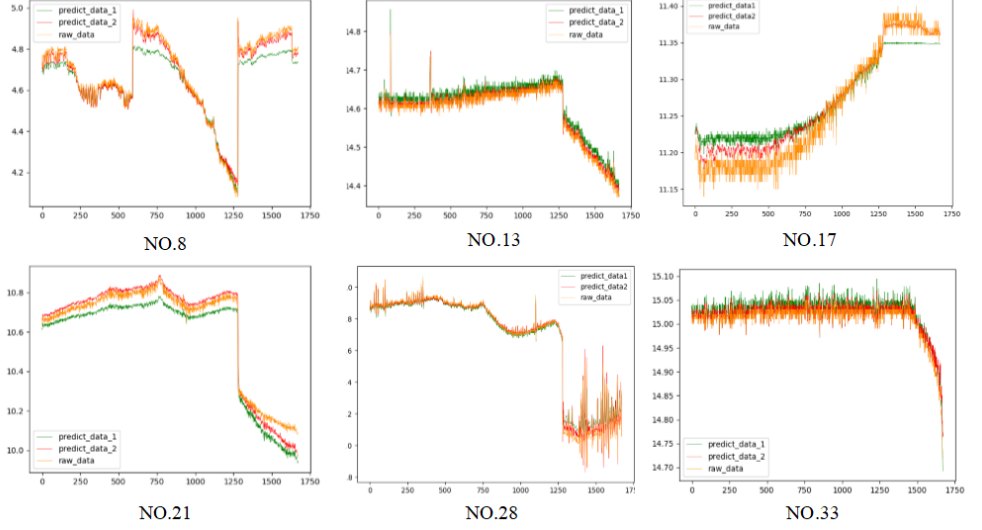


**Figure 7.** The prediction results of saturation line at different positions. The green line, red line, orange line represent the prediction value from  $CNN - LSTM^1$ , prediction value from  $CNN - LSTM^2$  and raw data, respectively. From the prediction result, we can see the  $CNN - LSTM^2$  outperform the  $CNN - LSTM^1$ .

**Table 2.** Prediction performance of the proposed  $CNN - LSTM^1$  model using MAPE, RMSE and  $R^2$ .

Metrics	NO.8	NO.13	NO.17	NO.21	NO.28	NO.33
RMSE	0.0214	0.0344	0.0491	0.0313	0.0134	0.0342
MAPE	3.814	4.411	3.731	3.242	3.712	3.621
$R^2$	0.885	0.756	0.851	0.702	0.913	0.865

$CNN - LSTM^1$  consists of two convolutional layers of 16 and 32, a max-pooling layer filters of 2, a LSTM layer of 50, a flatten layer and a fully-connected layer. While the  $CNN - LSTM^2$  includes one convolutional layer filters of 32, a max-pooling layer filters of 2, a flatten layer, two LSTM layers of 25, 50, a flatten layer and a fully-connected layer. From Table 2 and Table 3 combining with Figure 7, we can conclude that in terms of RMSE, MAPE and  $R^2$ , our proposed model  $CNN - LSTM^2$  outperform the  $CNN - LSTM^1$ . More specifically, the model which includes one convolutional layer, one max-pooling layer, a flatten layer, two LSTM layers, a flatten layer and a fully-connected layer is more accurate. In fact, even the convolutional layer is good at extraction and recognition, which could detect the spatial features of the saturation line value well. The deep and abstract features the convolutional layer learned may be different from the ordinary time-series information from the raw data. This is obviously a disadvantage when the monitoring data contains only simple information. While using one convolutional layer is more suitable and two LSTM layers can capture the long-short-term data dependencies to a significant degree from the result. The scatter plots of raw data and predicted saturation line is illustrated in Figure 8, which helps show the prediction performance more intuitively.

To show the superiority of our proposed model  $CNN - LSTM^2$ , we applied comparative studies with other state-of-the-art machine learning and deep learning models, including the support vector regression (SVR), decision tree regression (DTR), random forest regression (RFR), multilayer perception (MLP), single GRU, simple RNN

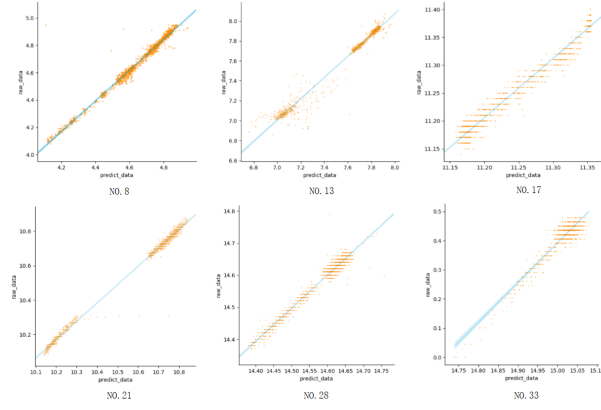


**Figure 8.** The prediction scatters of saturation line at different positions using  $CNN - LSTM^2$ .

**Table 3.** Prediction performance of the proposed  $CNN - LSTM^2$  model using MAPE, RMSE and  $R^2$ .

Metrics	NO.8	NO.13	NO.17	NO.21	NO.28	NO.33
RMSE	0.0209	0.030	0.0336	0.0170	0.0123	0.0366
MAPE	3.346	3.316	3.207	1.589	3.221	3.432
$R^2$	<b>0.969</b>	<b>0.974</b>	<b>0.937</b>	<b>0.981</b>	<b>0.951</b>	<b>0.892</b>

as well as LSTM models. Table 4 presents the RMSE, MAPE and  $R^2$  score of these models in our experiments, which demonstrates that our  $CNN - LSTM^2$  method significantly outperforms the others in  $R^2$ . Besides, the runtime for 120 epochs is much less than other deep learning models.

In order to build the complete saturation line prediction model and show the reliability of our CNN-LSTM<sup>2</sup> model together with parameters set, we compared different hyperparameters such as batch size, filters in of the convolutional layers, max-pooling size, number of LSTM cells in our experiments. Table 5 lists the different situations of combining multiple hyperparameters. In term of the evaluation metrics used in this task, although Case 2 and Case 5 achieve a little bit better performance than our model using ordinary hyperparameters in Case 9, the Runtime is almost twice the CNN-LSTM<sup>2</sup> model. Excessive running time will reduce the real-time performance of

**Table 4.** Performance comparison of different machine learning and deep learning models.

RMSE	MAPE	$R^2$	Runtime (second)	Model Type
0.132	4.542	0.548	—	SVR
0.141	4.312	0.489	—	DTR
0.251	4.186	0.839	—	RFR
—	—	—	—	—
0.0504	3.744	0.798	44.08	MLP
0.0308	3.645	0.864	47.54	RNN
0.0221	3.602	0.879	63.55	GRU
0.0214	3.596	0.887	77.08	LSTM
<b>0.0209</b>	<b>3.346</b>	<b>0.969</b>	<b>25.49</b>	<b>CNN-LSTM<sup>2</sup></b>

---

**Table 5.** Prediction cases using different hyperparameters in CNN-LSTM<sup>2</sup> model.

	Batch	Conv	Pool	LSTM	RMSE	MAPE	R <sup>2</sup>	Runtime
1	32	16	2	[25,50]	0.0411	3.352	0.899	50.87
2	<b>64</b>	<b>32</b>	<b>2</b>	<b>[50,75]</b>	<b>0.0208</b>	<b>3.324</b>	<b>0.971</b>	<b>49.37</b>
3	<b>32</b>	<b>16</b>	<b>4</b>	<b>[25,50]</b>	<b>0.0514</b>	<b>4.114</b>	<b>0.792</b>	<b>21.13</b>
4	64	32	4	[50,75]	0.0504	4.011	0.801	21.88
5	<b>16</b>	<b>16</b>	<b>2</b>	<b>[50,50]</b>	<b>0.0296</b>	<b>3.322</b>	<b>0.972</b>	<b>51.32</b>
6	128	16	4	[25,50]	0.0521	4.281	0.784	25.12
7	16	32	2	[25,75]	0.0385	3.513	0.902	50.52
8	128	32	2	[25,50]	0.0311	3.501	0.932	37.49
9*	<b>64</b>	<b>32</b>	<b>2</b>	<b>[25,50]</b>	<b>0.0209</b>	<b>3.346</b>	<b>0.969</b>	<b>25.49</b>

---

prediction, especially when the amount of data is very large. The disadvantage is more pronounced for a large amount of data, and this incurs no loss of generality. Case 3 need the least Runtime but achieve low accuracy. As a result, the CNN-LSTM<sup>2</sup> with one convolutional layer and two LSTM layers become the best performer. This is also in full compliance with deep learning logic. Although the padding method restricts the feature loss of the time-series data to some extent, the pooling layer inevitably loses part of the data information. Considering the accuracy and running time of the model, we keep the model parameters as same as the ordinary model. To be clear, the batch size is equal to 64, one convolutional layer filters of 32, a max-pooling layer filters of 2, two LSTM layers of 25 and 50. When the tailings ponds meet more complex situation, the data will become very complicated and internal time-series information is harder to calculate. At that time, single shallow deep learning layer lacks the capability to capture complex information and deeper layers of LSTM cells will be more suitable.

## Experiment and Results using Wavelet-CNN-LSTM model

After the above analysis and experiments, our CNN-LSTM model has achieved effective predictions in terms of infiltration line prediction. It can be seen from Figure 8 that the original data and the predicted data still do not satisfy the relationship between  $y = x$ , especially in the predictions NO17, NO.28, and NO.33. This is because although the long-term and short-term dependence and hidden time series information can be discovered from the data, the prediction accuracy is greatly affected due to the presence of noise in the data.

To overcome the drawbacks of CNN-LSTM<sup>2</sup> model that cannot de-noise the raw data, we applied the DWT to decompose the saturation line into different time-frequency sequences and remove the random noise. Subsequently, the data after noise reduction is trained by our CNN-LSTM<sup>2</sup> model. Our Wavelet-CNN-LSTM model is shown in Figure 10. The part A is the de-noise process using discrete wavelet transform, which removes the noise with small wavelet coefficients and the wavelet coefficients belonging to the useful signal are retained, making the data easier to extract to its local features. In part B, the de-noised data is feed to the CNN-LSTM<sup>2</sup> model for predicting the future tendency. The decomposition-denoise-reconstruction process of saturation line data is illustrated in Figure 9(a) and the original data (green) and de-noised data (orange) in different positions is illustrated in Figure9 (b). The results of all positions are shown in Figure 11. This once again proves that the DWT method can remove a large amount of useless information, thereby assisting our CNN-LSTM<sup>2</sup> model to more accurately explore the time series information hidden between the data. Table 6 presents the RMSE, MAPE and  $R^2$  comparing the CNN-LSTM<sup>2</sup> model with Wavelet-CNN-LSTM model. It can be illustrated from Table 6 that the Wavelet-CNN-LSTM model achieve the better performance than the CNN-LSTM<sup>2</sup>

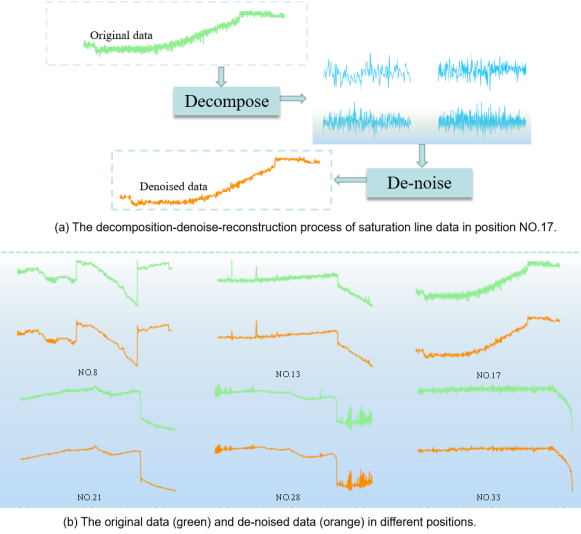


**Figure 9.** The decomposition-denoise-reconstruction process of saturation line data. It is obviously that after DWT process, the random noise of original data (green) is deleted and the data become smooth (orange).

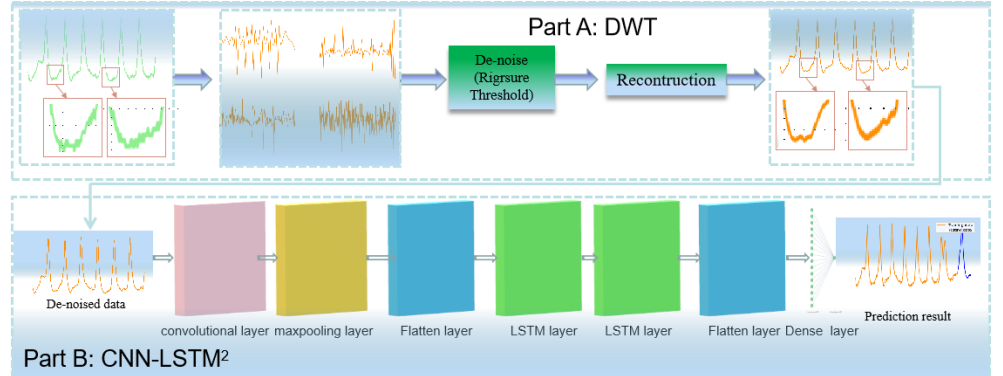


**Figure 10.** The Wavelet-CNN-LSTM model. The part A is the de-noise process. In part B, the de-noised data is feed to the CNN-LSTM<sup>2</sup> model for predicting.

model at all saturation line stations. After overcoming the shortcomings that the original CNN-LSTM<sup>2</sup> model cannot de-noise the data, our Wavelet-CNN-LSTM becomes the better choice for the prediction purpose.

## Discussion and Conclusion

In this work, we applied a new method to predict the safety of tailings pond according to the saturation line using *Wavelet – CNN – LSTM<sup>2</sup>* model, which is also first used in tailings pond risk prediction. Compared with the traditional methods, the risk evaluation method of tailings ponds has the characteristics of high accuracy and high real-time performance. The contributions of this work is four fold: Firstly, a NI system (including Pearson correlation coefficients, sensitivity analysis and random forest algorithms) was applied for reconstructing missing and abnormal values of saturation line by water level of the tailings pond and rainfall. It should be observed that the water level and rainfall have the same time-series information with saturation line at the same period. Secondly, two CNN-LSTM models, especially the *CNN – LSTM<sup>2</sup>* model

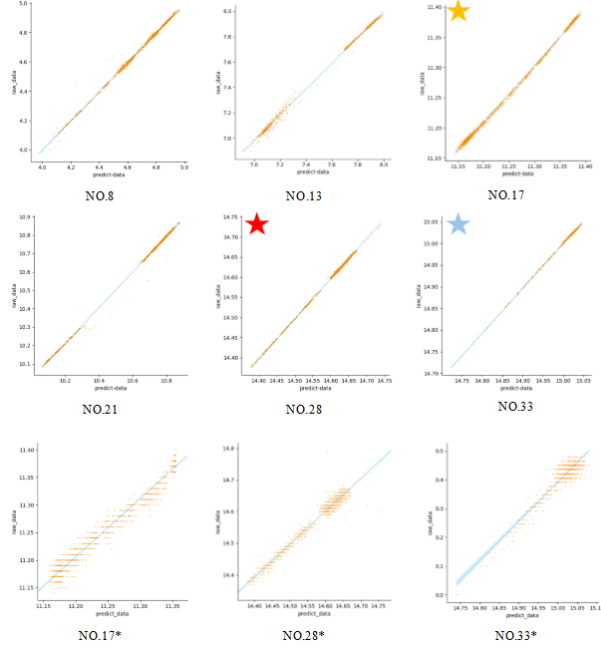


**Figure 11.** The prediction scatters of saturation line at different positions using Wavelet-CNN-LSTM<sup>2</sup> model. The prediction results of NO.17, NO.28, and NO.33 positions are respectively marked as yellow, red and blue, which obviously outperform the results (NO.17\*, NO.28\*, and NO.33\*) using the CNN-LSTM<sup>2</sup> model.

**Table 6.** Performance comparison of CNN-LSTM<sup>2</sup> and Wavelet-CNN-LSTM<sup>2</sup>.

Station	RMSE	MAPE	R <sup>2</sup>	Model Type
NO.8	0.0209	3.346	0.969	CNN-LSTM <sup>2</sup>
NO.8	0.0205	2.321	0.988	Wavelet-CNN-LSTM <sup>2</sup>
NO.13	0.0301	3.316	0.974	CNN-LSTM <sup>2</sup>
NO.13	0.0231	2.425	0.984	Wavelet-CNN-LSTM <sup>2</sup>
NO.17	0.0336	3.407	0.937	CNN-LSTM <sup>2</sup>
NO.17	0.0046	2.032	0.986	Wavelet-CNN-LSTM <sup>2</sup>
NO.21	0.0170	1.589	0.981	CNN-LSTM <sup>2</sup>
NO.21	0.0161	2.056	0.995	Wavelet-CNN-LSTM <sup>2</sup>
NO.28	0.0123	3.221	0.951	CNN-LSTM <sup>2</sup>
NO.28	0.0114	2.023	0.987	Wavelet-CNN-LSTM <sup>2</sup>
NO.33	0.0366	3.432	0.892	CNN-LSTM <sup>2</sup>
NO.33	0.0179	3.512	0.968	Wavelet-CNN-LSTM <sup>2</sup>

---

is shown to outperform other state-of-the-art models, such as SVR, DTR, RFR, MLP, RNN, GRU and LSTM. Conclusively, although these models can also achieve good performance, the  $CNN - LSTM^2$  still far ahead in RMSE, MAPE,  $R^2$ . Moreover, the Runtime of  $CNN - LSTM^2$  is another advantage, which is more pronounced in a larger amount of dataset. Thirdly, for a better understanding of the meaning of hyperparameters, we conducted more experiments using different batch size, convolutional layer filter size, max-pooling size and LSTM cell size. Fourthly, after a series of comparative experiments, we synthesized the best model  $CNN - LSTM^2$ . Based on this model, the wavelet transform method is applied to overcome the shortcomings that the original  $CNN - LSTM^2$  model could not de-noise the data. The wavelet transform decomposes the data into 4 layers of wavelets, selects the *rigrsure* threshold to de-noise the decomposed wavelets and then reconstructs them, subsequently feeds the reconstructed useful signals to our  $CNN - LSTM^2$  model to obtain better prediction results.

In tailings pond risk prediction task, these experiments consequently provide applicability of the Wavele-CNN-LSTM<sup>2</sup> model. It is worth mentioning that the Wavele-CNN-LSTM<sup>2</sup> model could also be applied in other time-series predictions including water level prediction, weather prediction and air quality prediction. It is evident that the model can not only to extract and recognize the structures in the time series and spatial features, but also identify long-term and short-term series information of the data.

In the future, we will focus on more factors of the safety monitoring parameters of the tailings pond, such as the underground displacement, ground displacement and dry beach length. Furthermore the risk level corresponding to the monitoring parameters of the tailings pond should be built to more intuitively reflect the safety of the tailings pond in our future work.

## References

1. World Information Service on Energy Uranium Project. Chronology of Major Tailings Dam Failures. Available online: <http://www.wiseuranium.org/mdaf.html> (accessed on 19 April 2019).
2. Zhai M G, Yang S F, Chen N H, et al. Big data epoch: Challenges and opportunities for geology[J]. Bulletin of Chinese Academy of Sciences, 2018, 33(8): 825-831.
3. Huang L, Miao F, Wang M X. Designing and setting up a monitoring and early warning system for tailings ponds in a region[J]. China Safety Science Journal, 2013, 23(12): 146-152.
4. Yang J, Sun Y, Li Q, et al. Measure Dry Beach Length of Tailings Pond Using Deep Learning Algorithm[C]//Proceedings of the 2019 International Conference on Robotics, Intelligent Control and Artificial Intelligence. 2019: 503-508.
5. Li Q, Tian W, Wang Y. Study on displacement analysis methods of tailing ponds on-line monitoring system[J]. Journal of Safety Science and Technology, 2011, 8: 47-52.
6. Yongzhi GAO, Yu CHU, Wei L. Remote sensing monitoring and analysis of tailings ponds in the ore concentration area of Heilongjiang Province[J]. Remote Sensing for Land & Resources, 2014, 27(1): 160-163.
7. Necsou M, Walter G R. Detection of uranium mill tailings settlement using satellite-based radar interferometry[J]. Engineering Geology, 2015, 197: 267-277.

- 
8. Che D, Liang A, Li X, et al. Remote sensing assessment of safety risk of iron tailings pond based on runoff coefficient[J]. *Sensors*, 2018, 18(12): 4373.
  9. Zhang J, Wu X, Zhao G. Study on Safety On-Line Monitoring and Warning Systems of Tailings Reservoir[M]//Electrical, Information Engineering and Mechatronics 2011. Springer, London, 2012: 589-598.
  10. Dong L, Shu W, Sun D, et al. Pre-alarm system based on real-time monitoring and numerical simulation using internet of things and cloud computing for tailings dam in mines[J]. *IEEE Access*, 2017, 5: 21080-21089.
  11. Qiu P, Yuan X, Gan S, et al. Monitoring System of Saturation Line Based on Mixed Programming[C]//2nd International Conference on Computer Engineering, Information Science & Application Technology (ICCIA 2017). Atlantis Press, 2016.
  12. Yang J, Wang W, Lin G, et al. Infrared Thermal Imaging-Based Crack Detection Using Deep Learning[J]. *IEEE Access*, 2019, 7: 182060-182077.
  13. WANG F, YANG K, XU Z, et al. Stability analysis of tailings dam based on saturation line matrix [J]. *Rock and Soil Mechanics*, 2009, 3.
  14. Chaoyang H E , Nengpan J U , Jian H . Automatic integration and analysis of multi-source monitoring data for geo-hazard warning[J]. *Journal of Engineering Geology*, 2014.
  15. code for design of tailings facilities (GB50863-2013), 2014.
  16. Mohri M, Rostamizadeh A, Talwalkar A. *Foundations of machine learning*[M]. MIT press, 2018.
  17. Ghoraani B , Krishnan S , Selvaraj R J , et al. Adaptive time-frequency signal analysis and its case study in biomedical ecgwaveform analysis[C]// International Conference on Digital Signal Processing. IEEE Press, 2009.
  18. Ghoraani B , Umapathy K , Sugavaneswaran L , et al. Pathological speech signal analysis using time-frequency approaches.[J]. *Critical Reviews in Biomedical Engineering*, 2012, 40(1):63-95.
  19. Ganguli S , Dunnmon J . Machine Learning for Better Models for Predicting Bond Prices[J]. *Papers*, 2017.
  20. Prochazka A , Sys V . Time series prediction using genetically trained wavelet networks[C]// Neural Networks for Signal Processing. IEEE, 2002.
  21. A. Prochazka. Neural networks and seasonal time-series prediction[C]// International Conference on Artificial Neural Networks. IET, 1997.
  22. Strobl C, Boulesteix A L, Zeileis A, et al. Bias in random forest variable importance measures: Illustrations, sources and a solution[J]. *BMC bioinformatics*, 2007, 8(1): 25.
  23. Shensa M J . The discrete wavelet transform: wedding the a trous and Mallat algorithms[J]. *IEEE Transactions on Signal Processing*, 2002, 40(10):P.2464-2482.
  24. Mokhtari A, Frey H C. Sensitivity analysis of a two-dimensional probabilistic risk assessment model using analysis of variance[J]. *Risk Analysis: An International Journal*, 2005, 25(6): 1511-1529.

- 
25. Kiparissides A, Kucherenko S S, Mantalaris A, et al. Global sensitivity analysis challenges in biological systems modeling[J]. *Industrial & Engineering Chemistry Research*, 2009, 48(15): 7168-7180.
26. Gilles J. Empirical Wavelet Transform[J]. *IEEE Transactions on Signal Processing*, 2013, 61(16):3999-4010.
27. Shentu N, Li Q, Li X, et al. Displacement parameter inversion for a novel electromagnetic underground displacement sensor[J]. *Sensors*, 2014, 14(5): 9074-9092.
28. Tseng F M, Yu H C , Tzeng G H . Combining neural network model with seasonal time series ARIMA model[J]. *Technological Forecasting and Social Change*, 2002, 69(1):71-87.
29. Chawla N V, Lazarevic A, Hall L O, et al. SMOTEBoost: Improving prediction of the minority class in boosting[C]//European conference on principles of data mining and knowledge discovery. Springer, Berlin, Heidelberg, 2003: 107-119.
30. Chawla N V, Bowyer K W, Hall L O, et al. SMOTE: synthetic minority over-sampling technique[J]. *Journal of artificial intelligence research*, 2002, 16: 321-357.
31. Altmann A, Tološi L, Sander O, et al. Permutation importance: a corrected feature importance measure[J]. *Bioinformatics*, 2010, 26(10): 1340-1347.
32. Huang F , Yin K , Huang J , et al. Landslide susceptibility mapping based on self-organizing-map network and extreme learning machine[J]. *Engineering Geology*, 2017, 223:11-22.
33. Faming H , Xiaoyan L , Weiping L . Stability Analysis of Hydrodynamic Pressure Landslides with Different Permeability Coefficients Affected by Reservoir Water Level Fluctuations and Rainstorms[J]. *Water*, 2017, 9(7):450.
34. Fiaschi S, Mantovani M, Frigerio S, et al. Testing the potential of Sentinel-1A TOPS interferometry for the detection and monitoring of landslides at local scale (Veneto Region, Italy)[J]. *Environmental Earth Sciences*, 2017, 76(14): 492.
35. Altai sky M . Continuous wavelet transform in quantum field theory[C]// *Frontiers of Fundamental Physics* 14. 2016.
36. Altai sky M V , Kaputkina N E . Continuous Wavelet Transform in Quantum Field Theory[J]. *Phys.rev.d*, 2013, 88(2):1235-1238.
37. Parra L, Sendra S, Lloret J, et al. Design and deployment of a smart system for data gathering in aquaculture tanks using wireless sensor networks[J]. *International Journal of Communication Systems*, 2017, 30(16): e3335.
38. Benesty J, Chen J, Huang Y, et al. Pearson correlation coefficient[M]//Noise reduction in speech processing. Springer, Berlin, Heidelberg, 2009: 1-4.
39. Benesty J, Chen J, Huang Y. On the importance of the Pearson correlation coefficient in noise reduction[J]. *IEEE Transactions on Audio, Speech, and Language Processing*, 2008, 16(4): 757-765.
40. Bergstra J, Bengio Y. Random search for hyper-parameter optimization[J]. *Journal of machine learning research*, 2012, 13(Feb): 281-305.

- 
41. Yang J, Sun Y, Li Q, et al. Effective Risk Prediction of Tailings Ponds Using Machine Learning[C]// 2020 3rd International Conference on Advanced Electronic Materials, Computers and Software Engineering (AEMCSE). 2020.
  42. Linda B , Soares J B P . The Influence of Tailings Composition on Flocculation[M]// The evolution of cognition /. MIT Press, 2015.
  43. Hariri-Ardebili M A , Pourkamali-Anaraki F . Support vector machine based reliability analysis of concrete dams[J]. Soil Dynamics and Earthquake Engineering, 2018, 104:276-295.
  44. Rankovic V , Grujovic N , Divac D , et al. Development of support vector regression identification model for prediction of dam structural behaviour[J]. Structural Safety, 2014, 48:33-39.
  45. Zhao H B . Slope reliability analysis using a support vector machine[J]. Computers & Geotechnics, 2008, 35(3):459-467.
  46. Cha Y J , Choi W , Oral Büyüköztürk. Deep Learning-Based Crack Damage Detection Using Convolutional Neural Networks[J]. Computer-Aided Civil and Infrastructure Engineering, 2017.
  47. Li J , Dai Q , Ye R . A novel double incremental learning algorithm for time series prediction[J]. Neural Computing and Applications, 2018.
  48. Cortez B , Carrera B , Kim Y J , et al. An architecture for emergency event prediction using LSTM recurrent neural networks[J]. Expert Systems with Applications, 2018, 97:315-324.
  49. Maragatham G , Devi S . LSTM Model for Prediction of Heart Failure in Big Data[J]. Journal of Medical Systems, 2019, 43(5).
  50. Lecun Y , Bengio Y . Convolutional Networks for Images, Speech, and Time-Series[J]. Handbook of Brain Theory & Neural Networks, 1995.
  51. Ronneberger O , Fischer P , Brox T . U-Net: Convolutional Networks for Biomedical Image Segmentation[J]. 2015.
  52. Hochreiter S , Schmidhuber J . Long Short-Term Memory[J]. Neural Computation, 1997, 9(8):1735-1780.